



Nanoscale

Nanoscale Light- and Voltage-Induced Lattice Strain in Perovskite Thin Films

Journal:	<i>Nanoscale</i>
Manuscript ID	NR-COM-10-2020-007476.R1
Article Type:	Communication
Date Submitted by the Author:	09-Dec-2020
Complete List of Authors:	Qiu, Haian; Binghamton University, Physics Mativetsky, Jeffrey; Binghamton University, Physics, Applied Physics and Astronomy

SCHOLARONE™
Manuscripts

COMMUNICATION

Nanoscale Light- and Voltage-Induced Lattice Strain in Perovskite Thin Films

Haian Qiu^a and Jeffrey M. Mativetsky^{*a}

Received 00th January 20xx,

Accepted 00th January 20xx

DOI: 10.1039/x0xx00000x

We report on localized nonlinear lattice deformation and nanoscale structural rearrangement in methylammonium lead triiodide films triggered by the combined action of light and voltage. These effects, revealed by second harmonic piezoresponse force microscopy, are connected with organic cation motion, implicating localized cation migration as a key contributor to perovskite optoelectronic device instability under operating conditions.

Introduction

Methylammonium lead halide perovskites have emerged as groundbreaking materials for a new generation of photovoltaics, photodetectors, and light emitting devices.¹⁻⁵ The power conversion efficiency of perovskite solar cells has risen dramatically, from 3.8% to beyond 25% within a decade.^{6, 7} The remarkable performance of perovskites has been attributed to a large optical absorption coefficient,⁸ tunable band gap,⁹ small exciton binding energy,^{10, 11} long carrier diffusion length,¹² and high defect tolerance.^{13, 14} Despite the unprecedented rapid progress in perovskite device performance, the intrinsic instability of methylammonium lead halide perovskite thin films has impeded their practical application. Owing to an inherently soft ionic crystal lattice, ionic migration can take place via Schottky defects (vacancies), Frenkel defects (interstitials), and grain boundaries (GBs).^{13, 15} Perovskite stability can also be impacted by external stimuli, such as illumination or electric field, that lead to defect formation,¹⁶ lattice disorder,¹⁷ increased ionic diffusion,¹⁸⁻²⁰ and eventual decomposition under prolonged illumination.²¹

Ionic motion within methylammonium lead halide perovskites is intimately linked with lattice strain. The methylammonium lead halide lattice consists of a three-

dimensional framework of inorganic lead halide octahedra and organic methylammonium cations (MA⁺) that occupy the voids between the octahedra. The MA⁺ and surrounding inorganic cage are strongly coupled through ionic interactions and hydrogen bonding between the methyl and amino groups of the MA⁺ and the halogen anions of the inorganic framework.²²⁻²⁵ As a result, changes in MA⁺ orientation produce a corresponding tilt of the inorganic framework.²² Under illumination, the binding energy between the MA⁺ and inorganic scaffold is reduced, leading to a higher degree of rotational and translational freedom of the MA⁺ and concomitant distortions of the inorganic lattice.^{26, 27} First principles simulations show that during MA⁺ migration, an opening of the inorganic framework is required for the cation to move between lattice sites.^{4, 28} Furthermore, according to density function theory simulations, because of the strong electric dipole moment of MA⁺,²⁴ under the combined effect of illumination and electric field, MA⁺ dipole alignment causes an expansion of the perovskite lattice.²⁷

Despite the predicted interdependence between lattice strain, ionic motion, and external stimuli such as light and electric field, little is known about the role of nanoscale morphology in mediating these effects. Scanning thermo-ionic microscopy (STIM) has recently been demonstrated as a means of mapping nanoscale ionic activity under local thermal excitation.^{29, 30} An alternative approach, piezoresponse force microscopy (PFM), has been applied to spatially map perovskite lattice strain in response to an applied AC voltage between a probe and sample.³¹⁻³³ The linear response between the applied voltage and resulting surface displacement in methylammonium lead halide perovskite samples has been associated with ferroelectric and ferroelastic phenomena.³⁴⁻³⁶ Although scarcely explored, it has been suggested that a second harmonic PFM response can arise from ionic redistribution.³⁷⁻³⁹ Using a spatially averaged PFM approach, Huang and coworkers recently reported on a macroscopic second harmonic electromechanical response from methylammonium lead triiodide (MAPbI₃) single crystals under low frequency AC bias.⁴⁰

^a Department of Physics, Applied Physics and Astronomy, Binghamton University, Binghamton, New York, 13902, USA

*E-mail: jmativet@binghamton.edu

†Electronic Supplementary Information (ESI) available: [details of any supplementary information available should be included here]. See DOI: 10.1039/x0xx00000x

It was suggested that the observed strain was caused by a bias-induced formation of Frenkel defects. To date, the second harmonic PFM response, which holds potential for probing higher order lattice strain induced by ionic motion, has not been spatially mapped in methylammonium lead halide perovskite films. Insight into the spatial distribution of nonlinear lattice strain triggered by light and voltage is promising for providing a window into the role of localized ion migration in perovskite degradation and device performance hysteresis.⁴¹⁻⁴⁵

In this study, we investigate the interplay between ionic motion and nanoscale localized lattice strain due to external stimuli, i.e., illumination and voltage bias, in MAPbI₃ perovskite thin films. By spatially and temporally resolving lattice strain using PFM, we observe a pronounced lateral second harmonic strain response at low AC bias frequencies that increases with light exposure time and preferentially resides at GBs and nearby regions. The emergence of surface protrusions following concurrent light and voltage bias conditions points to localized MA⁺ motion in the vicinity of GBs that produce irreversible structural transformations. These results implicate MA⁺ migration as a key mechanism for instability in methylammonium lead halide perovskite optoelectronic devices under voltage bias and light.

Results and discussion

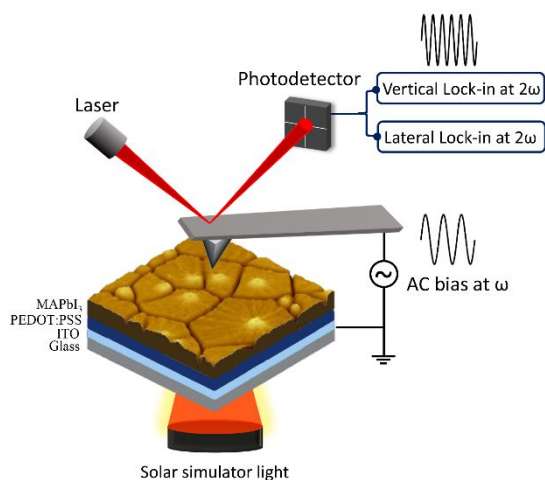


Figure 1. Schematic showing the sample configuration and experimental setup used for second harmonic strain mapping.

Figure 1 shows the setup used for strain response mapping. The sample comprised a 300 nm thick MAPbI₃ thin film fabricated on a poly(2,3-dihydrothieno-1,4-dioxin)-poly(styrenesulfonate) (PEDOT:PSS)-coated indium tin oxide (ITO) substrate, a typical configuration used in inverted perovskite solar cells. Tetragonal phase MAPbI₃ perovskite thin films (Supplementary Information, Figure S1) were deposited through a two-step process in a nitrogen-filled glovebox and shown to exhibit a photovoltaic response (see Supplementary Information, Section 1 and Figure S2).⁴⁶ The Pt-coated probe was maintained in contact with the sample while an AC bias

with an amplitude of 2 V and frequency of 0.8 kHz was applied to the probe to induce periodic mechanical displacements at the perovskite surface. Vertical and lateral second harmonic oscillations of the cantilever were detected and recorded simultaneously with topography.

We first tracked the second harmonic strain as a function of light exposure time, as shown in Figure 2. Measurements were performed in a nitrogen-filled glovebox to exclude the influence of oxygen or moisture. The simultaneously recorded cantilever deflection (Figure 2a) shows a polycrystalline film structure, with terracing within the grains and a grain size that varies from 100 nm to 500 nm. The deflection signal tracks deviations from the deflection setpoint and is more sensitive to topographic changes than height measurements, which can be seen in the Supplementary Information, Figure S3. Under dark conditions (Figure 2b), the lateral second harmonic strain exhibits a weak contrast. After 5 min of light soaking, using solar simulator light with an irradiance of 4500 W/m², a strain map was recorded at the same sample location under continuous illumination (Figure 2c). These measurements reveal a pronounced, heterogeneous strain response, with the strongest response concentrated at or near most GBs. As the light soaking time was increased to 30 min and 60 min (Figure 2d and 2e, respectively), the contrast between GBs and grain interiors saturates.

It should be noted that the measured second harmonic strain contrast was entirely lateral, with the vertical strain amplitude maps showing no distinguishable features under dark or light conditions (see Supplementary Information, Figure S3). We found that the strain was most pronounced at low AC bias frequencies (1 kHz and below) and became negligible at 5 kHz and above (Supplementary Information, Figure S5). We also observed reproducible lateral second harmonic strain under forward and reverse scan directions, confirming that the features are unrelated to scanning artefacts (Supplementary Information, Figure S6). Furthermore, when switching the illumination off and on during strain map acquisition (Supplementary Information, Figure S4), we saw that the lateral second harmonic strain abruptly drops, within seconds, and then gradually recovers after re-illumination, demonstrating the reversibility of the light-induced strain. The rapid dissipation of the strain when the light is turned off suggests that it is the illumination itself, rather than light-induced heat buildup, that softens the lattice.

Nanoscale second harmonic electromechanical coupling between the biased probe and surface can arise from multiple mechanisms, including: electrostatic capacitive forces between the probe and charge near the sample surface,^{47, 48} Coulombic attractive stress (Maxwell stress) due to oppositely charged surfaces of the film,⁴⁹ induced polarization (electrostriction),^{50, 51} and thermal expansion due to Joule heating.^{52, 53} For insight into the nanoscale capacitive interactions between the probe and sample, we performed scanning capacitance microscopy (SCM) measurements under noncontact conditions (Supplementary Information, Figure S7).⁵⁴ The resulting SCM maps show no differences in the capacitive signals recorded under dark and 30 min light exposure conditions. We therefore rule out capacitive forces resulting from charge accumulation as

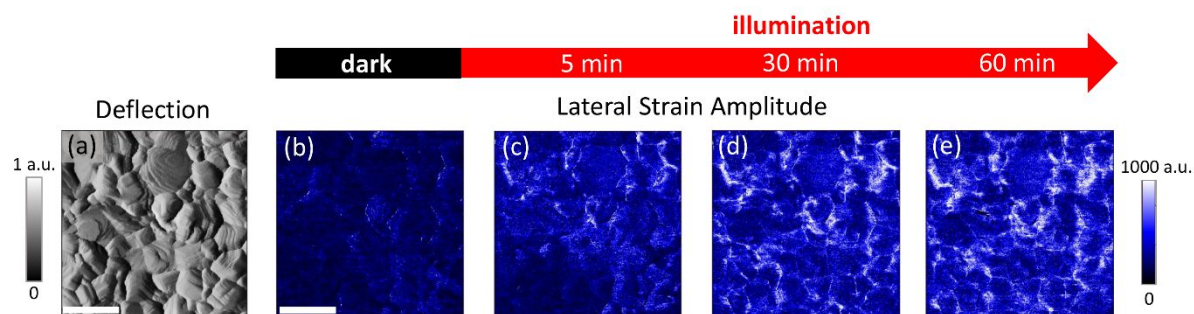


Figure 2. (a) Cantilever deflection and (b–e) lateral second harmonic strain amplitude images: (b) under dark conditions and following illumination for (c) 5 min, (d) 30 min, and (e) 60 min. Each image took about 10 min to record and was scanned from bottom to top. The scale bars represent 600 nm.

the cause of the observed light-induced second harmonic PFM strain signal. It should also be noted that induced polarization occurs on a much faster timescale (e.g., microseconds),⁴⁰ compared to the millisecond timescale of the strain response recorded here. Moreover, electrostriction caused by induced polarization exhibits an increased response with contact force,⁵² which is not the case in our measurements (see Supplementary Information, Figure S8).

Thermal expansion due to current-induced Joule heating could also result in a pronounced second harmonic PFM signal at low AC voltage frequencies.^{52, 53} Although the volume expansion due to Joule heating is quadratically dependent on voltage, we found a weaker dependence of lateral second harmonic strain amplitude on voltage (Supplementary Information, Figure S9). Above 3V, the strain became more uniformly distributed and saturated. The lateral second harmonic strain was also acquired with an additional DC bias added to the probe (on-field measurement) to induce current flow and the resulting strain was suppressed (see Supplementary Information, Figure S11); conversely, an enhanced strain would be expected for Joule heating.⁵³ Furthermore, volume expansion caused by local heating should be relatively isotropic and would therefore not produce the observed lateral strain contrast without a similar accompanying vertical signal. For these reasons, we exclude Joule heating as a cause for the observed nonlinear lateral strain. The lack of vertical nonlinear strain contrast also indicates that volumetric expansion caused by ion buildup (Vegard strain) is not taking place; in cases where Vegard strain occurs, PFM is commonly referred to as electrochemical strain microscopy (ESM).^{55, 56}

To explain the observed second lateral harmonic strain, we look to the strong coupling between ionic motion and lattice distortion in methylammonium lead halide perovskites. Several details about the observed second harmonic strain support such a mechanism. Firstly, the lattice deformation under light stimulus is most pronounced near GBs which serve as channels for ion migration in perovskite thin films.^{57–59} The reduced coordination of ions at GBs and the higher concentration of vacancies and other defects near GBs make these regions susceptible to lattice distortion^{60–62} that can accommodate ion flow and produce a pronounced PFM strain signal. Secondly, the response to light exposure evolves over a timescale of minutes,

similar to light soaking effects associated with ion redistribution in perovskite solar cells.^{63–67} Third, the cutoff AC bias frequency for a nonlinear strain response (≤ 1 kHz) is close to the hopping rate for MA⁺ within methylammonium lead halide perovskites and much lower than the rate for halide migration.^{68–72} At higher AC voltage frequencies, slowly migrating ions may not keep up with the frequency of the alternating electric field, resulting in a reduced lattice distortion and strain signal. Fourth, the second harmonic strain is lateral, caused by in-plane perovskite lattice distortion. This in-plane distortion can be caused by lateral stretching of the inorganic framework as the ions are driven to oscillate vertically by the applied electric field.²⁸ The nonlinear response would stem from lateral lattice stretching taking place as ions displace in response to a positive and negative bias, i.e. twice per cycle.

GBs serve as the main ion migration pathways when the AC bias amplitude is at or below 2 V. This observation is consistent with STIM measurements of thermally-induced ionic strain in MAPbI₃.^{29, 30} At higher voltages, we see increased ionic activity within grains, with Schottky defects likely playing a role in ion transport (see Supplementary Information, Figure S9).^{28, 73}

In principle, any of the constituent ions (I⁻, MA⁺, and Pb²⁺) can migrate within the perovskite films. Computationally and experimentally-determined activation energies for ion migration reveal that I⁻ (0.34 eV) is the most mobile ionic species, followed by MA⁺ (0.70 eV) and Pb²⁺ (1.56 eV), which is far less mobile. The activation energies are estimated based on average values across nine studies.⁷⁴ Due to the higher

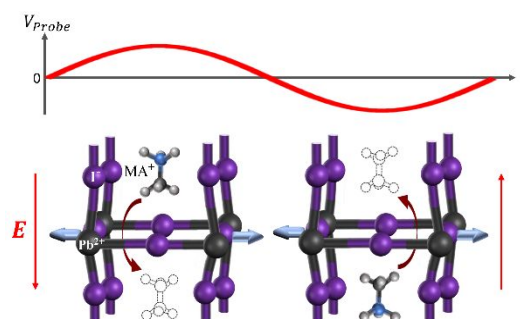


Figure 3. Proposed scheme for lateral second harmonic strain caused by MA⁺ alignment and hopping under AC bias and illumination.

activation energy of MA⁺ compared with I⁻, MA⁺ migration was

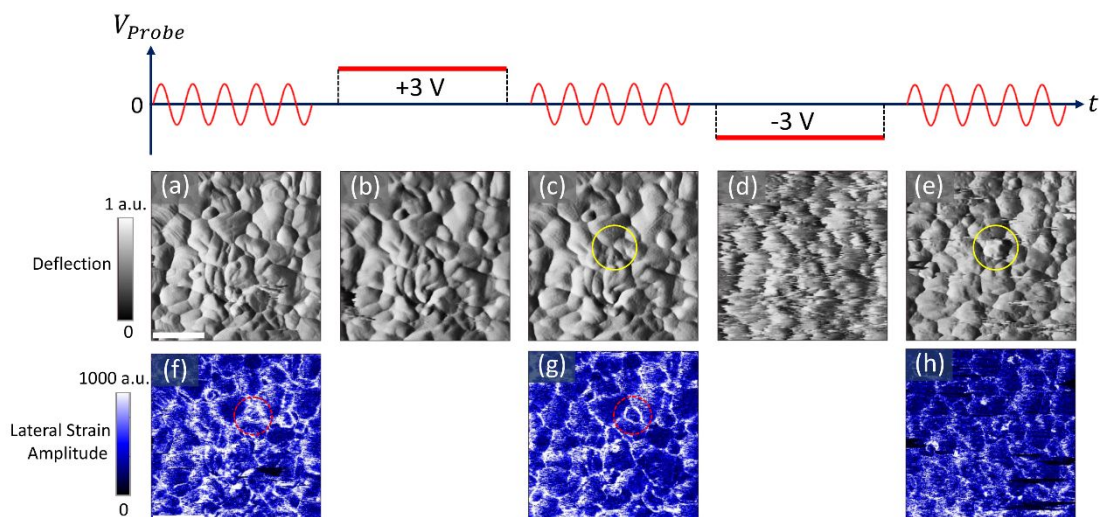


Figure 4. (a, c, e) Deflection and (f, g, h) lateral second harmonic strain amplitude images obtained under illumination; (a) was recorded after 30 minutes of light soaking. (b, d) Deflection images obtained with contact mode AFM under illumination with (b) +3 V and (d) -3 V applied to the probe. The scale bars represent 600 nm. The solid yellow circles in (c) and (e) indicate a local change in morphology after the application of a -3 V DC bias. The dashed red circles in (f) and (g) highlight an example of a local change in strain response after the application of a +3 V DC bias.

demonstrated to be more strongly dependent on illumination.^{26, 75} Another way to distinguish between MA⁺ and I⁻ migration is that the processes occur on different time scales. A first-principles computational study by Angelis *et al.* predicted that iodine-related defects migrate through a 300 nm thick perovskite film on much shorter time scales than MA vacancies (<1 μ s versus tens of ms).⁷¹ The characteristic timescale in our strain measurements is thus more consistent with MA⁺ ion migration. Furthermore, based on molecular dynamics simulations, Meloni and coworkers showed that halide migration causes a much smaller lattice distortion than MA⁺ cations, which requires an opening of the inorganic framework to hop between lattice sites.²⁸ Therefore, although I⁻ migration likely occurs during our measurements (due to a low activation energy for transport), the halide anions will not cause an appreciable lattice strain during second harmonic PFM mapping.

In light of the above arguments, we hypothesize that light-induced MA⁺ ion migration under bias is the primary contribution to the observed lateral second harmonic surface deformation. In addition to the second harmonic lattice strain caused by ion hopping, structural relaxation of the inorganic cage will take place when the MA⁺ reaches a new site and further lattice distortion will occur as MA⁺ dipoles align with the oscillating electric field;²⁷ these effects may add to the observed lattice response. The proposed ion-migration-induced process for lateral second harmonic lattice strain is illustrated in Figure 3.

To test this hypothesis, we mapped the lateral second harmonic strain before and after applying a DC bias, as shown in Figure 4. First, deflection and strain (Figure 4a, f) were recorded under illumination, following 30 minutes of light soaking. Next, the AC probe bias was turned off and a +3 V DC bias was applied while measuring the deflection in contact

mode (Figure 4b). A DC bias should cause ion depletion or accumulation at the sample surface, depending on the relative sign of the bias and ionic species. We then recorded, once again, the deflection and strain (Figure 4c, g). The strain map before and after a +3 V bias are highly similar, showing an enhanced response at GBs and nearby regions. Careful observation, nevertheless, reveals local changes in the strain image, for example, as indicated with the dashed red circles in Figure 4f and g. In this case, the lateral strain signal became more sharply defined at the GBs after the application of a positive DC bias. This result suggests that the MA⁺ ions drifted away from the surface under positive bias and then diffused back, but not necessarily along the same pathways, resulting in a redistribution of MA⁺.

Interestingly, when the DC bias is switched to -3 V, the topography (Supplementary Information, Figure S13) and deflection (Figure 4d) exhibit extensive streaks, which can be caused by diffusing or loosely bound objects being pushed around by the AFM probe during scanning.^{76, 77} We propose that under a -3 V probe bias, MA⁺ ions are pulled to the sample surface, leading to the observed streaks. Some streaks are still

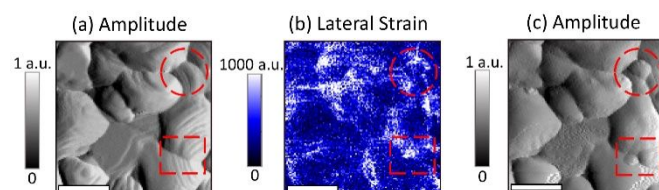


Figure 5. Consecutive (a) tapping mode amplitude, (b) lateral second harmonic strain amplitude, and (c) tapping mode amplitude measured on a perovskite film. The circle and square outlines indicate regions where morphological changes occur following strain mapping. The scale bars represent 300 nm. The strain measurements were performed under illumination, following 30 min of light soaking. The tapping mode measurements were performed in the dark.

visible in the deflection image after the -3 V DC bias was

switched off, indicating that not all of the displaced ions have returned to a stable configuration (Figure 4e). In addition, the emergence of new protrusions at the surface can be seen, for example, within the highlighted yellow region in Figure 4e. These protrusions form above GBs, where there is increased ion flow. This result supports the notion that MA⁺ ion migration to the perovskite surface leads to nanoscale structural rearrangement. Owing to the low mobility of Pb²⁺, we speculate that the protrusions consist of MAI, which is consistent with the observed increase in carbon content and decrease in iodide in similarly formed bias-induced structures.⁷⁸ Measurements performed under dark conditions (shown in Supplementary Information, Figure S12) exhibit a greatly reduced strain signal and a far weaker streaking effect under a negative DC bias, confirming that light facilitates the MA⁺ migration.

To decouple potential effects of scanning the AFM probe in contact with the sample surface from the combined effects of an applied AC field and light, we performed less invasive intermittent contact (tapping mode) measurements before and after strain mapping (Figure 5). Similar to the deflection signal in contact mode, the cantilever amplitude recorded during tapping mode is more sensitive to surface features than height measurements. As shown in Figure 5a and 5c, recorded before and after strain mapping, there are two notable features: (1) new protrusions are formed near GBs, and (2) terraces seen before strain mapping become smoothed afterwards. It should be noted that a DC bias was not used to accumulate charge near the surface. In this case, the AC bias and light during strain mapping induced protrusion formation. Careful comparison between Figure 5b and 5c reveals that the locations where small protrusions emerge (Figure 5c) coincide with locations bearing a higher lateral second harmonic strain response (Figure 5b), as marked with red circles and squares. These measurements suggest that regions with increased MA⁺ migration activity are more prone to light and bias-induced morphological change. Furthermore, these results implicate nanoscale structural rearrangement induced by light- and bias-activated MA⁺ movement as likely sources of perovskite instability and device degradation.

It should be noted that the smoothing of the terraced structure within grains during PFM mapping also occurs during contact mode imaging without an applied bias or light (see Supplementary Information, Figure S15 and S16), indicating that the soft perovskite lattice is susceptible to subtle polishing during sliding contact with the AFM probe. The emergence of new protrusions, however, was only observed following bias and light exposure.

Conclusions

To conclude, higher harmonic PFM is promising for investigating links between electric field-induced nonlinear mechanical strain, ionic motion, and film stability. In this study, nanoscale second harmonic strain mapping was used to visualize localized nonlinear lateral lattice strain near GBs in MAPbI₃ thin films upon combined exposure to light and AC bias. The strain increases over the course of minutes and is most prominent at

bias frequencies under 1 kHz. Measurements following the application of a DC bias support the role of MA⁺ cation migration in the observed strain response. We propose that under the combined action of light and an AC bias, light reduces the energetic barrier for MA⁺ migration, while the AC bias induces vertical cation movement, predominantly near GBs. In-plane lattice opening to accommodate MA⁺ hopping results in the lateral second harmonic strain seen in our measurements. We also observe that cation motion under light and bias can induce lattice instability and mass transport, leading to the formation of surface protrusions near GBs that serve as channels for ion transport. Given the sensitivity of local photocurrent and power conversion in perovskite solar cells to grain structure and composition,⁷⁹ local irreversible changes in structure at the perovskite surface are expected to have a significant and irreversible impact on device performance.

These results show the intimate connection between MA⁺ flow, lattice strain, and structural stability in methylammonium lead halide perovskites. This work also bolsters the case for MA⁺ movement under light and voltage bias as a source of structural and performance instability in optoelectronic devices based on these materials. Strategies for reducing cation migration and improving perovskite stability, which can benefit from nanoscale ionic strain characterization, include morphology engineering to reduce GB density,⁸⁰ GB passivation,⁸¹ composition engineering,⁸² and interfacial strain mitigation.^{36,83}

Author contributions

HQ performed experiments and analysed data. HQ and JMM designed experiments, interpreted results, and wrote the paper. JMM supervised the study.

Conflicts of interest

There are no conflicts to declare.

Acknowledgements

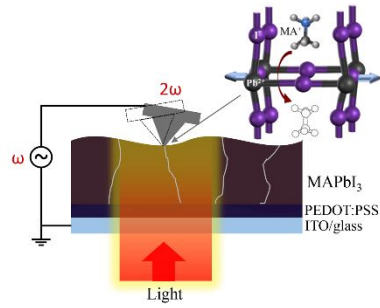
We gratefully acknowledge support from the National Science Foundation (CAREER award DMR-1555028).

References

1. J. Huang, Y. Yuan, Y. Shao and Y. Yan, *Nature Reviews Materials*, 2017, **2**, 17042.
2. M. Yuan, L. N. Quan, R. Comin, G. Walters, R. Sabatini, O. Voznyy, S. Hoogland, Y. Zhao, E. M. Beauregard, P. Kanjanaboos, Z. Lu, D. H. Kim and E. H. Sargent, *Nature Nanotechnology*, 2016, **11**, 872-877.
3. P. Liu, W. Wang, S. Liu, H. Yang and Z. Shao, *Adv. Energy Mater.*, 2019, **9**, 1803017.
4. A. K. Jena, A. Kulkarni and T. Miyasaka, *Chem. Rev.*, 2019, **119**, 3036-3103.
5. L. Dou, Y. M. Yang, J. You, Z. Hong, W. H. Chang, G. Li and Y. Yang, *Nat. Commun.*, 2014, **5**, 5404.

6. A. Kojima, K. Teshima, Y. Shirai and M. T., *J. Am. Chem. Soc.*, 2009, **131**, 6050-6051.
7. NREL, Best Research-Cell Efficiency Chart, <https://www.nrel.gov/pv/cell-efficiency.html> (accessed August 15, 2020, 2020).
8. W. J. Yin, J. H. Yang, J. Kang, Y. Yan and S. H. Wei, *J. Mater. Chem. A*, 2015, **3**, 8926-8942.
9. W. J. Yin, T. Shi and Y. Yan, *Adv. Mater.*, 2014, **26**, 4653-4658.
10. K. Galkowski, A. Mitioglu, A. Miyata, P. Plochocka, O. Portugall, G. E. Eperon, J. T. Wang, T. Stergiopoulos, S. D. Stranks, H. J. Snaith and R. J. Nicholas, *Energy Environ. Sci.*, 2016, **9**, 962-970.
11. K. Wang, D. Yang, C. Wu, M. Sanghadasa and S. Priya, *Progress in Materials Science*, 2019, **106**, 100580.
12. S. D. Stranks, G. E. Eperon, G. Grancini, C. Menelaou, M. J. P. Alcocer, T. Leijtens, L. M. Herz, A. Petrozza and H. J. Snaith, *Science*, 2013, **342**, 341-344.
13. W. J. Yin, T. Shi and Y. Yan, *Appl. Phys. Lett.*, 2014, **104**, 063903.
14. J. Kim, S. H. Lee, J. H. Lee and K. H. Hong, *J. Phys. Chem. Lett.*, 2014, **5**, 1312-1317.
15. D. Meggiolaro, E. Mosconi and F. D. Angelis, *ACS Energy Lett.*, 2019, **4**, 779-785.
16. S. T. Birkhold, J. T. Precht, R. Giridharagopal, G. E. Eperon, L. Schmidt-Mende and D. S. Ginger, *J. Phys. Chem. C*, 2018, **122**, 12633-12639.
17. D. Kim, J. S. Yun, P. Sharma, D. S. Lee, J. Kim, A. M. Soufiani, S. Huang, M. A. Green, A. W. Y. Ho-Baillie and J. Seidel, *Nat. Commun.*, 2019, **10**, 444.
18. Y. Yuan, J. Chae, Y. Shao, Q. Wang, Z. Xiao, A. Centrone and J. Huang, *Adv. Energy Mater.*, 2015, **5**, 1500615.
19. E. Mosconi, D. Meggiolaro, H. J. Snaith, S. D. Stranks and F. D. Angelis, *Energy Environ. Sci.*, 2016, **9**, 3180-3187.
20. J. Haruyama, K. Sodeyama, L. Han and Y. Tateyama, *J. Am. Chem. Soc.*, 2015, **137**, 10048-10051.
21. A. F. Akbulatov, L. A. Frolova, N. N. Dremova, I. Zhidkov, V. M. Martynenko, S. A. Tsarev, S. Y. Luchkin, E. Z. Kurmaev, S. M. Aldoshin, K. J. Stevenson and P. A. Troshin, *J. Phys. Chem. Lett.*, 2020, **11**, 333-339.
22. L. Z. Tan, F. Zheng and A. M. Rappe, *ACS Energy Lett.*, 2017, **2**, 937-942.
23. O. Yaffe, Y. Guo, L. Z. Tan, D. A. Egger, T. Hull, C. C. Stoumpos, F. Zheng, T. F. Heinz, L. Kronik, M. G. Kanatzidis, J. S. Owen, A. M. Rappe, M. A. Pimenta and L. E. Brus, *Phys. Rev. Lett.*, 2017, **118**, 136001.
24. C. J. Tong, W. Geng, O. V. Prezhdo and L. M. Liu, *ACS Energy Lett.*, 2017, **2**, 1997-2004.
25. M. T. Weller, O. J. Weber, P. F. Henry, A. M. Di Pumpo and T. C. Hansen, *Chem. Commun.*, 2015, **51**, 4180-4183.
26. M. Bag, L. A. Renna, R. Y. Adhikari, S. Karak, F. Liu, P. M. Lahti, T. P. Russell, M. T. Tuominen and D. Venkataraman, *J. Am. Chem. Soc.*, 2015, **137**, 13130-13137.
27. R. Gottesman, E. Haltzi, L. Gouda, S. Tirosh, Y. Bouhadana, A. Zaban, E. Mosconi and F. D. Angelis, *J. Phys. Chem. Lett.*, 2014, **5**, 2662-2669.
28. S. Meloni, T. Moehl, W. Tress, M. Franckevicius, M. Saliba, Y. H. Lee, P. Gao, M. K. Nazeeruddin, S. M. Zakeeruddin, U. Rothlisberger and M. Graetzel, *Nat. Commun.*, 2016, **7**, 10334.
29. E. N. Esfahani, A. Eshghinejad, Y. Ou, J. Zhao, S. Adler and J. Li, *Microscopy Today*, 2017, **25**, 12-19.
30. J. Li, B. Huang, E. N. Esfahani, L. Wei, J. Yao, J. Zhao and W. Chen, *npj Quantum Materials*, 2017, **2**, 56.
31. H. Röhm, T. Leonhard, M. J. Hoffmann and A. Colmann, *Energy Environ. Sci.*, 2017, **10**, 950-955.
32. H. S. Kim, S. K. Kim, B. J. Kim, K. S. Shin, M. K. Gupta, H. S. Jung, S. W. Kim and N. G. Park, *J. Phys. Chem. Lett.*, 2015, **6**, 1729-1735.
33. Z. Fan, J. Xiao, K. Sun, L. Chen, Y. Hu, J. Ouyang, K. P. Ong, K. Zeng and J. Wang, *J. Phys. Chem. Lett.*, 2015, **6**, 1155-1161.
34. S. M. Vorpahl, R. Giridharagopal, G. E. Eperon, I. M. Hermes, S. A. L. Weber and D. S. Ginger, *ACS Appl. Energy Mater.*, 2018, **1**, 1534-1539.
35. Y. Liu, L. Collins, R. Proksch, S. Kim, B. R. Watson, B. Doughty, T. R. Calhoun, M. Ahmadi, A. V. Ievlev, S. Jesse, S. T. Retterer, A. Belianinov, K. Xiao, J. Huang, B. G. Sumpter, S. V. Kalinin, B. Hu and O. S. Ovchinnikova, *Nat. Mater.*, 2018, **17**, 1013-1019.
36. E. Strelcov, Q. Dong, T. Li, J. Chae, Y. Shao, Y. Deng, A. Gruverman, J. Huang and A. Centrone, *Sci. Adv.*, 2017, **3**, e1602165.
37. G. Xia, B. Huang, Y. Zhang, X. Zhao, C. Wang, C. Jia, J. Zhao, W. Chen and J. Li, *Adv. Mater.*, 2019, **31**, e1902870.
38. P. Wang, J. Zhao, L. Wei, Q. Zhu, S. Xie, J. Liu, X. Meng and J. Li, *Nanoscale*, 2017, **9**, 3806-3817.
39. Q. N. Chen, Y. Ou, F. Ma and J. Li, *Appl. Phys. Lett.*, 2014, **104**, 242907.
40. B. Chen, T. Li, Q. Dong, E. Mosconi, J. Song, Z. Chen, Y. Deng, Y. Liu, S. Ducharme, A. Gruverman, F. D. Angelis and J. Huang, *Nat. Mater.*, 2018, **17**, 1020-1026.
41. G. Richardson, S. E. J. O'Kane, R. G. Niemann, T. A. Peltola, J. M. Foster, P. J. Cameron and A. B. Walker, *Energy Environ. Sci.*, 2016, **9**, 1476-1485.
42. B. Chen, M. Yang, S. Priya and K. Zhu, *J. Phys. Chem. Lett.*, 2016, **7**, 905-917.
43. W. Tress, N. Marinova, T. Moehl, S. M. Zakeeruddin, M. K. Nazeeruddin and M. Grätzel, *Energy Environ. Sci.*, 2015, **8**, 995-1004.
44. H. J. Snaith, A. Abate, J. M. Ball, G. E. Eperon, T. Leijtens, N. K. Noel, S. D. Stranks, J. T. Wang, K. Wojciechowski and W. Zhang, *J. Phys. Chem. Lett.*, 2014, **5**, 1511-1515.
45. R. S. Sanchez, V. Gonzalez-Pedro, J. W. Lee, N. G. Park, Y. S. Kang, I. Mora-Sero and J. Bisquert, *J. Phys. Chem. Lett.*, 2014, **5**, 2357-2363.
46. Z. Xiao, Q. Dong, C. Bi, Y. Shao, Y. Yuan and J. Huang, *Adv. Mater.*, 2014, **26**, 6503-6509.
47. E. A. Eliseev, A. N. Morozovska, A. V. Ievlev, N. Balke, P. Maksymovych, A. Tselev and S. V. Kalinin, *Appl. Phys. Lett.*, 2014, **104**, 232901.
48. F. Johann, Á. Hoffmann and E. Soergel, *Physical Review B*, 2010, **81**.
49. Q. M. Zhang, H. Li, M. Poh, F. Xia, Z. Y. Cheng, H. Xu and C. Huang, *Nature*, 2002, **419**, 284-287.
50. S. M. Yang, M. B. Okatan, M. P. Paranthaman, S. Jesse, T. W. Noh and S. V. Kalinin, *Appl. Phys. Lett.*, 2014, **105**, 193106.
51. R. E. Newnham, V. Sundar, R. Yimnirun, J. Su and Q. M. Zhang, *J. Phys. Chem. B*, 1997, **101**, 10141-10150.
52. R. K. Vasudevan, N. Balke, P. Maksymovych, S. Jesse and S. V. Kalinin, *Appl. Phys. Rev.*, 2017, **4**, 021302.
53. N. Balke, S. Jesse, Q. Li, P. Maksymovych, M. Baris Okatan,

- E. Strelcov, A. Tselev and S. V. Kalinin, *J. Appl. Phys.*, 2015, **118**, 072013.
54. C. C. Williams, J. Slinkman, W. P. Hough and H. K. Wickramasinghe, *Appl. Phys. Lett.*, 1989, **55**, 1662-1664.
55. N. Balke, S. Jesse, A. N. Morozovska, E. Eliseev, D. W. Chung, Y. Kim, L. Adamczyk, R. E. García, N. Dudney and S. V. Kalinin, *Nature Nanotechnology*, 2010, **5**, 749-754.
56. N. Balke, S. Jesse, Y. Kim, L. Adamczyk, A. Tselev, I. N. Ivanov, N. J. Dudney and S. V. Kalinin, *Nano Lett.*, 2010, **10**, 3420-3425.
57. Y. Shao, Y. Fang, T. Li, Q. Wang, Q. Dong, Y. Deng, Y. Yuan, H. Wei, M. Wang, A. Gruverman, J. Shield and J. Huang, *Energy Environ. Sci.*, 2016, **9**, 1752-1759.
58. J. W. Lee, S. H. Bae, N. De Marco, Y. T. Hsieh, Z. Dai and Y. Yang, *Materials Today Energy*, 2018, **7**, 149-160.
59. Y. Yuan and J. Huang, *Acc. Chem. Res.*, 2016, **49**, 286-293.
60. R. Bennewitz, S. Schar, V. Barwich, O. Pfeiffer, M. Meyer, F. Krok, B. Such, J. Kolodziej and M. Szymonski, *Surface Science*, 2001, **474**, L197-L202.
61. V. V. Puchin, A. Shluger, Y. Nakai and N. Itoh, *Phys. Rev. B*, 1994, **49**, 11364-11373.
62. Y. Wang, W. H. Fang, R. Long and O. V. Prezhdo, *J. Phys. Chem. Lett.*, 2019, **10**, 1617-1623.
63. T. Zhang, S. H. Cheung, X. Meng, L. Zhu, Y. Bai, C. H. Y. Ho, S. Xiao, Q. Xue, S. K. So and S. Yang, *J. Phys. Chem. Lett.*, 2017, **8**, 5069-5076.
64. J. Hu, R. Gottesman, L. Gouda, A. Kama, M. Priel, S. Tirosh, J. Bisquert and A. Zaban, *ACS Energy Lett.*, 2017, **2**, 950-956.
65. M. Pazoki, T. J. Jacobsson, J. Kullgren, E. M. Johansson, A. Hagfeldt, G. Boschloo and T. Edvinsson, *ACS Nano*, 2017, **11**, 2823-2834.
66. C. Zhao, B. Chen, X. Qiao, L. Luan, K. Lu and B. Hu, *Adv. Energy Mater.*, 2015, **5**, 1500279.
67. D. W. deQuilettes, W. Zhang, V. M. Burlakov, D. J. Graham, T. Leijtens, A. Osherov, V. Bulovic, H. J. Snaith, D. S. Ginger and S. D. Stranks, *Nat. Commun.*, 2016, **7**, 11683.
68. K. Domanski, B. Roose, T. Matsui, M. Saliba, S. H. Turren-Cruz, J. P. Correa-Baena, C. R. Carmona, G. Richardson, J. M. Foster, F. De Angelis, J. M. Ball, A. Petrozza, N. Mine, M. K. Nazeeruddin, W. Tress, M. Grätzel, U. Steiner, A. Hagfeldt and A. Abate, *Energy Environ. Sci.*, 2017, **10**, 604-613.
69. J. Y. Seo, T. Matsui, J. Luo, J. P. Correa-Baena, F. Giordano, M. Saliba, K. Schenk, A. Ummadisingu, K. Domanski, M. Hadadian, A. Hagfeldt, S. M. Zakeeruddin, U. Steiner, M. Grätzel and A. Abate, *Adv. Energy Mater.*, 2016, **6**, 1600767.
70. J. P. Correa-Baena, M. Anaya, G. Lozano, W. Tress, K. Domanski, M. Saliba, T. Matsui, T. J. Jacobsson, M. E. Calvo, A. Abate, M. Grätzel, H. Miguez and A. Hagfeldt, *Adv. Mater.*, 2016, **28**, 5031-5037.
71. J. M. Azpiroz, E. Mosconi, J. Bisquert and F. D. Angelis, *Energy Environ. Sci.*, 2015, **8**, 2118-2127.
72. D. Yang, W. Ming, H. Shi, L. Zhang and M. Du, *Chem. Mater.*, 2016, **28**, 4349-4357.
73. C. Eames, J. M. Frost, P. R. Barnes, B. C. O'Regan, A. Walsh and M. S. Islam, *Nat. Commun.*, 2015, **6**, 7497.
74. T. Zhang, C. Hu and S. Yang, *Small Methods*, 2020, **4**, 1900552.
75. Y. Liu, N. Borodinov, M. Lorenz, M. Ahmadi, S. V. Kalinin, A. V. Ievlev and O. S. Ovchinnikova, *Adv. Sci.*, 2020, **7**, 2001176.
76. S. A. Burke, J. M. Mativetsky, R. Hoffmann and P. Grutter, *Phys. Rev. Lett.*, 2005, **94**, 096102.
77. M. Bohringer, W. D. Schneider and R. Berndt, *Surface Science* 1998, **408**, 72-85.
78. J. S. Yun, J. Seidel, J. Kim, A. M. Soufiani, S. Huang, J. Lau, N. J. Jeon, S. I. Seok, M. A. Green and A. Ho-Baillie, *Adv. Energy Mater.*, 2016, **6**, 1600330.
79. Y. Kutes, Y. Zhou, J. L. Bosse, J. Steffes, N. P. Padture and B. D. Huey, *Nano Lett.*, 2016, **16**, 3434-3441.
80. W. Nie, H. Tsai, R. Asadpour, J. C. Blancon, A. J. Neukirch, G. Gupta, J. J. Crochet, M. Chhowalla, S. Tretiak, M. A. Alam, H. Wang and A. D. Mohite, *Science*, 2015, **347**, 522-525.
81. T. Niu, J. Lu, R. Munir, J. Li, D. Barrit, X. Zhang, H. Hu, Z. Yang, A. Amassian, K. Zhao and S. F. Liu, *Adv. Mater.*, 2018, **30**, e1706576.
82. N. J. Jeon, J. H. Noh, W. S. Yang, Y. C. Kim, S. Ryu, J. Seo and S. I. Seok, *Nature*, 2015, **517**, 476-480.
83. J. Zhao, Y. Deng, H. Wei, X. Zheng, Z. Yu, Y. Shao, J. E. Shield and J. Huang, *Sci. Adv.*, 2017, **3**, eaao5616.



Combined light and voltage stimulus triggers localized cation migration, nonlinear lattice deformation, and nanoscale structural rearrangement in perovskite films providing insight into perovskite optoelectronic device instability.